The Feel System is an Extension of Both the Vehicle and Neuromuscular Systems

Edward Bachelder, edward.n.bachelder@nasa.gov, San Jose State University Research Foundation/ US Army Aviation Development Directorate, NASA Ames Research Center, Moffett Field, CA, USA.

Bimal Aponso, bimal.l.aponso@nasa.gov, Aeronautics Projects Office, NASA Ames Research Center,Moffett Field, CA, USA.

Abstract

In an aircraft with powered controls, a manual tracking task employs limb neuromuscular (NM) control of an inceptor, which can then provide input to a control system through an artificial feel system. Traditionally inceptors have been passive and hand-gripped, and the resulting inceptor-limb dynamics allowed the open-loop NM element to be represented as a self-contained second-order transfer function with a fixed damping ratio and natural frequency. However, active inceptors and gaming devices present themselves as candidate human-vehicle interfaces, and it is shown through elementary mechanical modeling how limb-inceptor interaction can influence the NM system. A physical example of this is provided. It is well-established that inceptor force feedback is an important NM cue to the pilot. An experiment using a passive joystick with and without spring restoring force investigated the effect of force feedback on tracking performance and NM response. The preliminary results suggest the role of NM equalization changes depending on whether force feedback is present, and that the presence or absence of force feedback influences the role of visual equalization. When it is available, force (rather than stick deflection) appears to be the signal employed to close the loop around the NM element. Neurophysiological research and this work's observations suggest that muscle tension arising from limb co-contraction drives operator gain, which in turn governs crossover frequency. This muscle tension affects the mechanical NM response by changing the muscle stiffness and damping. This work proposes a NM model that first integrates both limb and inceptor dynamics, from which the open-loop NM system can then be isolated using the feel system dynamics and loop closure made with the force output. The location of the NM mode can have a key influence on the extent that an operator can generate frequency compensation, and the degree to which the Crossover Model is adhered to.

1. NEUROMUSCULAR MODEL DEVELOPMENT: A HISTORICAL OVERVIEW

One of the earliest investigations of the role of the human neuromuscular system during manual tracking was documented in 1952 by Goodyear Aircraft (Ref. 1), where an operator's response (manipulator displacement) to tracking a step input was fitted to a transfer function. In Figure 1 (taken from Ref. 2) the solid lines fitted to the dotted responses were generated by the third-order transfer function given by Eqn. 1

$$Y_n = \frac{Ke^{-\tau s}\,\omega_n^2}{(s^3 + 2\zeta_n\omega_n s^2 + \omega_n^2 s + K\omega_n^2)} \qquad (1)$$

Y_n was given the appellate "neuromuscular system" in 1957 by McRuer (Figure *2*, taken from Ref. 2) as he observed both nerves and muscles were involved. Reaction time is denoted as a pure time delay τ, and the damping and frequency terms ζ_n and ω_n associated with the observed data in Figure 1 were 0.5 and 23.8, respectively.

Eleven years later experimentation at Systems Technology Inc. (STI) confirmed the third-order neuromuscular operator dynamics using sum-of-sines as a forcing function (Ref. 3). In this 1968 report

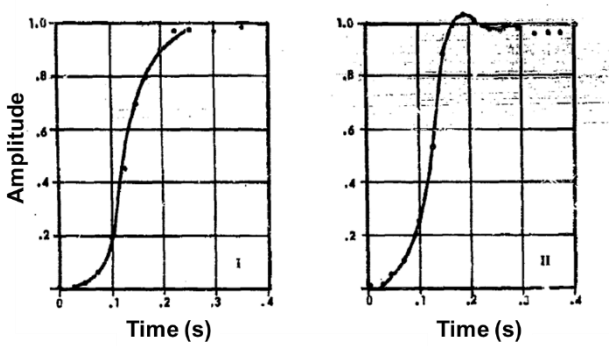

Figure 1. Two subject responses (dots) to identical step inputs and third-order fits (solid line) (Ref. 2).

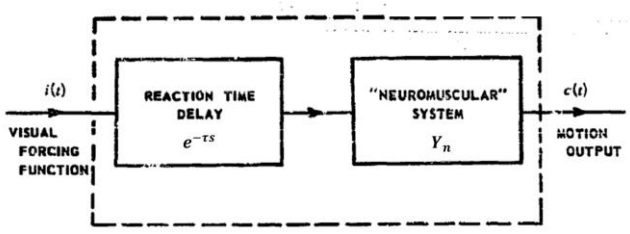

Figure 2. Block diagram representing neuromuscular response during a visual tracking task (Ref. 2).

Presented at 47th European Rotorcraft Forum, United Kingdom, 7-9th September 2021

the effects on the neuromuscular (NM) response due to inceptor characteristics such as inertia and spring restraint were examined using the apparatus shown in Figure 3.

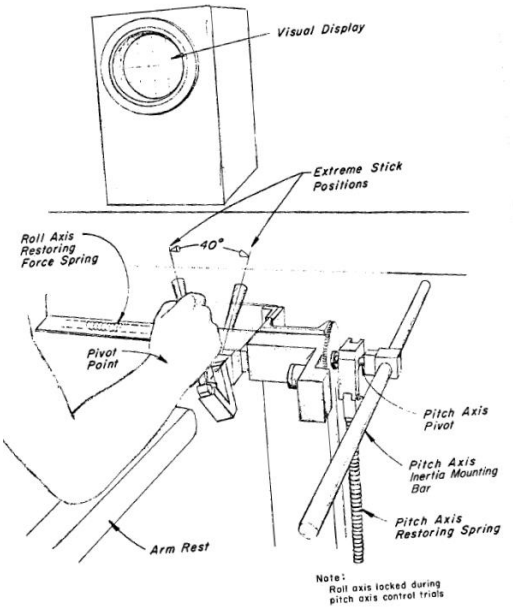

Figure 3. Experimental manipulator setup (Ref. 3).

In Ref. 4 McRuer proposed a NM actuation system model which contained two key developments: 1) the variation in system parameters as a function of average muscle tension or operating point; and 2) the role of the muscle spindle both as an equalization element and in its effects on muscle tone or average tension. The muscle spindle system was modeled using a combination of equivalent springs and dampers, an approach which was later extended to mechanically describe limb-feel system (FS) interaction. In Ref. 4 "feel system" referred to the lumped manipulator-artificial feel system suite, and this definition of FS is likewise adopted in this paper.

Magdaleno (Ref. 5) depicted position-sensing control (i.e., the vehicle is commanded via manipulator position) using nested force and position feedback loops shown in Figure 4. Here, force and position sensing elements augment the NM command signal generated by the equalization element G_e operating on the visual error signal.

In 1971 Magdaleno and McRuer (Ref. 6) further developed NM modeling concepts, wherein spindle and joint sensing respectively provided force and position feedback, shown in Figure 5. Here, the NM system adapts to the feel system (manipulator), where that the limb and FS dynamics are combined in a single element.

Figure 6 (taken from Ref. 6) is a diagram representing the muscle and manipulator elements, where the muscle characteristics consist of a force

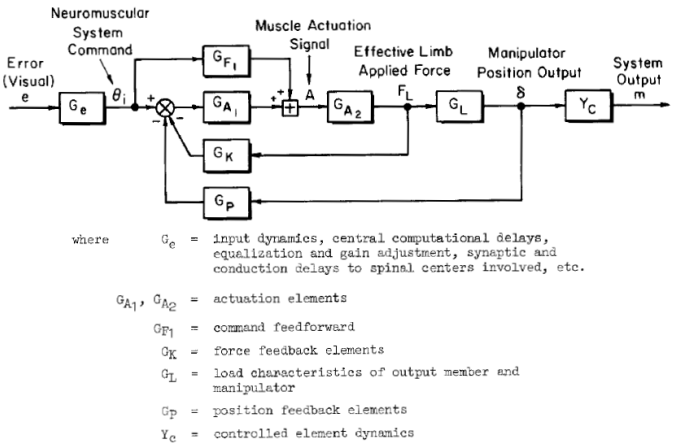

Figure 4. Feedback system for position-sensing control (Ref. 5).

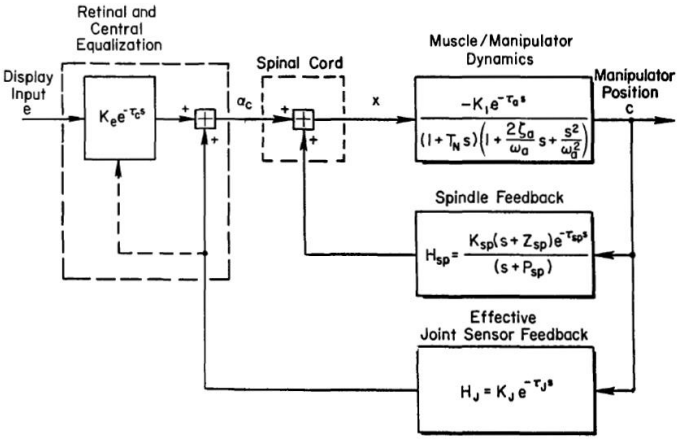

Figure 5. Neuromuscular subsystems for free moving and pressure manipulators and central equalization for rate dynamics (Ref. 6).

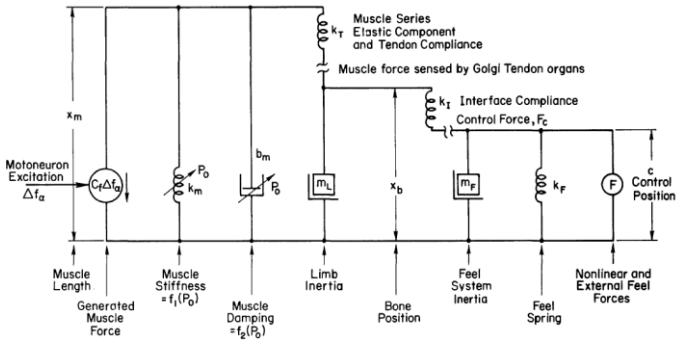

Figure 6. Muscle-manipulator elements (Ref. 6).

source plus spring k_m and damper b_m where the latter two tend to increase with operating point tension, P_o. The muscle model also has series elastic component which has been lumped into k_T, the tendon compliance. The tendon compliance is connected to the limb inertia, m_L, and to k_I, the interface compliance between the bone and the

Presented at 47th European Rotorcraft Forum, United Kingdom, 7-9th September 2021

manipulator handle (i.e., skin and flesh of the hand). The FS load is shown as an inertia m_F and spring k_F plus a force source to account for external disturbance forces and/or nonlinear FS properties.

The first study of the human operator as a linear servomechanism is that of Tustin (Ref. 7) who proposed that, despite amplitude nonlinearities, temporal discontinuities and haphazard fluctuations, there might be an "appropriate linear law" that would describe the main part of the operator's behavior. Insight from servomechanical design led McRuer (Ref.8) to develop the ubiquitous human crossover model (*CM*), where the pilot employs lead and lag equalization via the visual channel to adapt to the vehicle dynamics being controlled. With the *CM*, a variable pilot time delay can be used to explain phenomena such as increased high-frequency phase lag associated with increased amounts of error lead equalization. Smith (Ref. 9) first proposed the role of inner-loop rate feedback to support control of the error loop during compensatory tracking, whereby the operator visually sensed the rate of the controlled system's output. This manner of feedback was subject to two key constraints. The first being the bandwidth and noise characteristics associated with human visual sensing of rate, and secondly low ratio of disturbance-to-system-output, without which the error rate sensed by the operator will not correspond to system output rate. A realizable method for sensing rate for use with inner-loop feedback was posed by Hess (Ref. 10), whereby the operator employs kinesthetic sensing of control rate and an internal model of system response to that rate. This approach was later incorporated into Hess' Structural Model (*SM*) of the human pilot (Refs. 11, 12). Building on Krendel and McRuer's (Ref. 13) successive organization of perception (SOP) model for tracking skill development, Hess' pilot *SM* provides an integrated architecture for describing compensatory, pursuit, precognitive, and off-nominal behavior.

1. HESS' STRUCTURAL MODEL OF THE HUMAN PILOT

Hess (Ref. 10) proposed a model (Figure 7) for human compensatory tracking whose essential features included an outer loop operating on error (*e*), an inner feedback loop operating on stick deflection (δ), pilot elements that equalize the error and stick signals (respectively Y_{Pe}, $Y_{p_{\dot{m}}}$), a pilot element Y_{Pn} generating the NM force of the particular limb which drives the manipulator, the manipulator dynamics Y_δ that produces the vehicle input from the force command, a controlled element Y_c representing the vehicle dynamics, and the display element Y_d that transforms the physical system error to the displayed error being tracked. A disturbance *d* is added to the vehicle output *m*, and the negative of this is the error that the operator is attempting to null.

From Ref. 8 the NM element can be approximated by Eqn (1):

$$Y_{Pn} = \frac{\omega_n^2}{(S^2 + 2\zeta_n\omega_n + \omega_n^2)} \quad (1)$$

With the inner loop of Figure 7 closed, the simple quadratic form for Y_{Pn} can exhibit the key features of measured high-frequency human controller dynamics, namely, a typically subcritical damping ratio $\zeta_{n_{CL}}$, and a second-order amplitude fall-off beyond the undamped natural frequency $\omega_{n_{CL}}$. The injected remnant signal n_e is included to account for nonlinearities and/or time variations in quasilinear fashion.

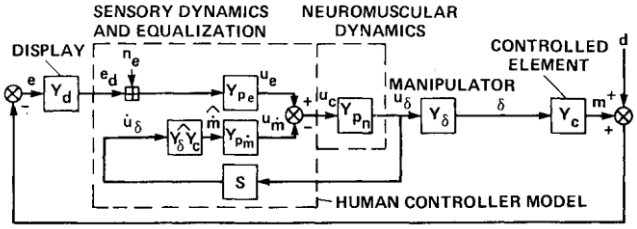

Figure 7. Quasilinear dual-loop model of the human controller (Ref. 10).

The main function of the inner-loop is to provide vehicle output rate feedback and improve stability and precision. Hess proposed that the NM force output is sensed and transformed into an estimate of vehicle output rate using an internal model of the manipulator and vehicle dynamics suite. For acceleration command dynamics, this process effectively requires the pilot to integrate the force output (in the dual-loop model shown the pilot first senses the force rate and integrates this twice). Hess hypothesized that proportional or derivative control in the feedback loop can be conducted using direct sensing from the muscle spindles and Golgi tendon organs (Ref. 14), but integral control does not have analogous sensing and requires the operator to employ higher-level cognition. Thus, when operating acceleration command systems, the pilot will tend to generate a pulsive force output rather than a continuous one since cognitively integrating the former is less difficult. "Ease of integrability" can be generally interpreted in a physiological sense as applying to those waveforms whose integration requires a minimum of higher-level activity in the central nervous system (Ref. 15).

As an operator becomes familiar with the vehicle and manipulator, the transformation between force output and vehicle output rate should reduce to a one-step process. In his revised *SM* (Ref. 16), Hess reflects this simplification with a proprioceptive feedback element, Y_{PF}, shown in Figure 8. This element receives stick position and depending on the vehicle

dynamics in the vicinity of the crossover frequency, Y_{PF} will assume one of the forms shown in Table 1.

Table 1. Proprioceptive feedback element Y_{PF} form.

Vehicle Dynamics	K_v	K_v/s	K_v/s^2
Y_{PF}	$K_\delta(s+a)$	K_δ	$K_\delta/(s+a)$

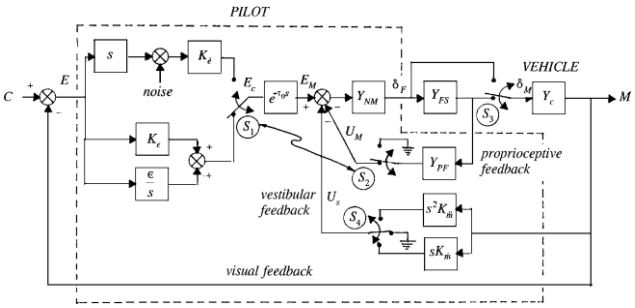

Figure 8. Structural Model of the Human Pilot (Ref. 16).

A gain K_e serves as the pilot element acting on error, and the NM and FS elements are respectively denoted by Y_{NM} and Y_{FS}. The central processing time delay τ_o, is approximated as invariant (0.20 seconds). The remaining elements of the *SM* are described in Ref. 16.

McRuer's modeling of the operator placed responsibility for lead/lag compensation with the Retinal and Central Equalization element (Figure 5), whereas Hess maintained it was conducted proprioceptively via force feedback.

One of the objectives of this research was to determine where equalization takes place, and under which conditions.

2. PROPOSED MODIFICATIONS TO THE STRUCTURAL MODEL

Bachelder in Ref. 17 conducted a single-axis simulation tracking task using proportional, rate, acceleration, and jerk command dynamics (a gamepad was employed as the inceptor). Using the simple lead-lag pilot model (Ref. 18) shown in Eqn. 2 to estimate pilot parameters, the identified slope at crossover of the open-loop (display-pilot-vehicle) system and operator pure time delay for the four command types are shown in Figure 9 and Figure 10, respectively.

$$Y_p = K_p \frac{(s+\omega\_\mathrm{Ld})}{(s+\omega\_\mathrm{Lg})} e^{-\tau s} \qquad (2)$$

It is seen that for dynamics other than rate command the slope at crossover departs significantly ($p < .01$)

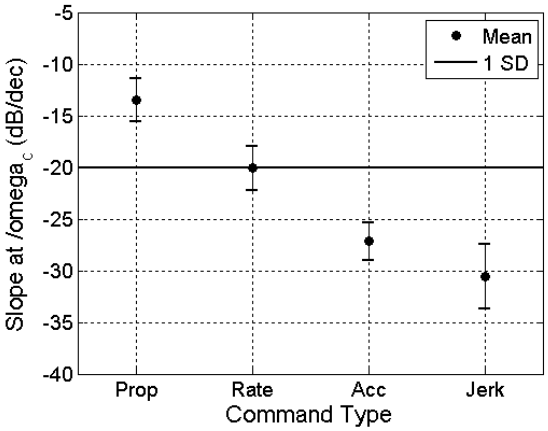

Figure 9. Open-loop gain slope at ω_c by command type using lead-lag pilot model (Ref. 19).

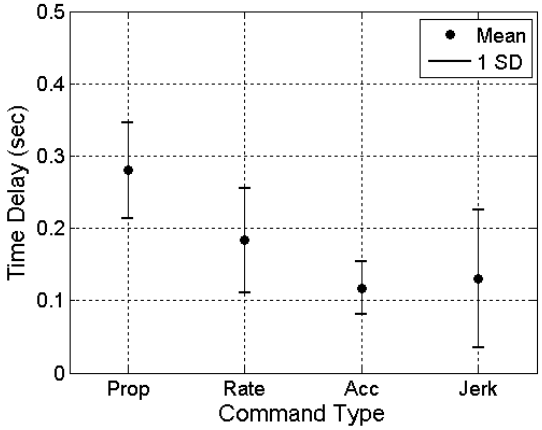

Figure 10. Time delay by command type using lead-lag pilot model (Ref. 20).

from the nominal -20 dB/decade value nominally attributed to the Crossover Model.

Three observations can be made regarding the Structural Model's format for the proprioceptive feedback element given in Table 1:

1. Vehicle dynamics can be encountered that do not neatly fall into one of the three categories. Furthermore, complex dynamics may undergo substantial change across frequency (relevant when crossover frequency shifts).
2. The absence of a counterbalancing lag and lead for the proportional and rate command conditions, respectively, assumes no upper bounds on operator lead and lag generation. Actual constraints on compensation can have considerable effect on closed-loop stability and performance, depending on the command dynamics.
3. Using the Crossover Model's nominal open-loop slope of -20 dB/decade to govern

selection of the lead or lag frequency *a* in Table 1will produce increasingly erroneous phase margin as the actual slope (Figure 9) deviates from the assumed nominal slope.

A generalized format for the proprioceptive feedback element G_{PF} is proposed in Eqn. (*3*, where K_{PF}, ω_Ld_{PF}, and ω_Lg_{PF} are the proprioceptive gain, lead and lag, respectively.

$$G_{PF} = K_{PF}\frac{(s+\omega\_Ld_{PF})}{(s+\omega\_Lg_{PF})} \quad (3)$$

In Ref. 21 Bachelder showed that the observed trend between operator processing time delay and command type seen in Figure 10 was required for a linear relationship between phase margin (PM) and perceived workload. PM-workload linearization enables a straightforward transformation of workload to PM, allowing a reference PM to be set by the pilot to facilitate loop control. The pilot processing time delay τ_o should thus be variable rather than fixed.

Finally, it will be shown later that the operator employs force feedback when it is available rather than the stick deflection signal, thus the NM element Y_{NM} in Figure 8 should use δ_F for feedback.

3. MUSCLE CO-CONTRACTION AND TRACKING PERFORMANCE

During manual tracking tasks associated with aircraft control, at a minimum there will be an agonist - antagonist muscle pair (Ref. 6) where each has an average tension. For motion to occur, one muscle must relax while the other contracts, and thus the tension levels must seesaw about an average. Co-contraction (COC) of agonist-antagonist muscles is commonly observed when performing difficult motor tasks (Ref. 22). The benefit of COC is thought to derive from increased muscle stiffness, enabling near-zero delay corrections to unexpected disturbances.

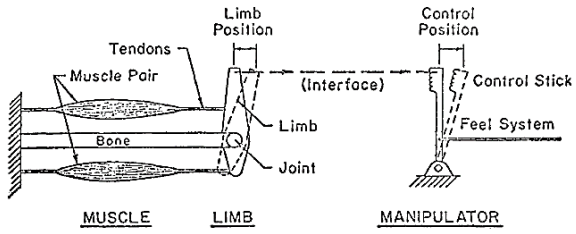

Figure 11. Idealized agonist/antagonist muscle pair (Ref. 6).

Reference 23 investigated the effect of COC on target tracking performance. The target moved at a constant speed along a trajectory that required only elbow flexion or extension. Once the end of the trajectory was reached, the target reversed direction and followed the same trajectory back to the starting point. At a random time, when the target was near the center of the trajectory, a perturbation torque pulse flexed or extended the elbow, displacing the fingertip from the target. Participants were instructed to perform the task with and without active antagonistic COC of the muscles spanning the elbow.

COC produced significantly better performance (Figure 12), reducing deviations from the desired elbow motion caused by the perturbation regardless of the movement and perturbation directions and eliminated overshoot at the end of the corrective response. Critically, the study showed that a dual agonist-antagonist control strategy improved performance even at low levels of COC.

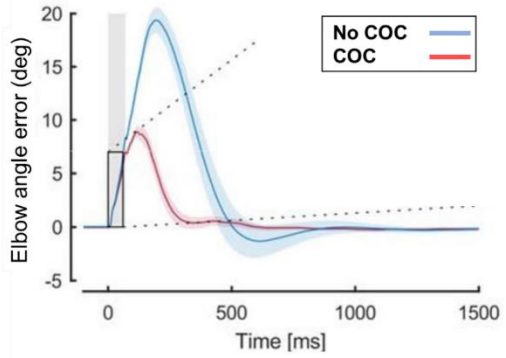

Figure 12. Elbow angle deviation from the target trajectory following mechanical perturbations without (blue) and with (red) active co-contraction (Ref. 23).

Another study (Ref. 22) varied tracking difficulty to investigate the influence of performance with varying COC. In Figure 13 COC was significantly correlated to tracking accuracy.

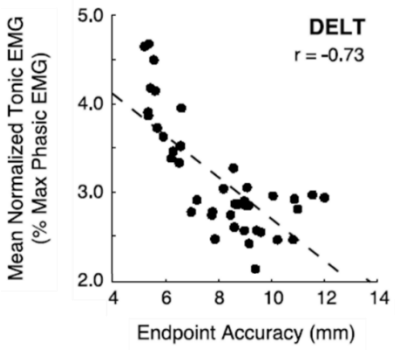

Figure 13. Direct relationship between cocontraction (deltoid muscle) during movement and accuracy. (Ref. 22).

In 2013 Delft University (Ref. 24) conducted research whose main objective was to study how NM feedback changed with varying manual control tasks. While the identified changes in NM feedback were anticipated,

the high levels of COC measured were not predicted as the researchers expected COC to be both inefficient and fatiguing. However, as the demand for precision increased, COC was observed to likewise increase.

4. NEUROMUSCULAR-MANIPULATOR DYNAMICS MODELING

The equations of motion for the lumped muscle-manipulator element shown in Figure 5 and Figure 6 can be found by setting the total force at the datums $c, x_b,$ and x_m equal to zero. In terms of Laplace transforms and written in matrix form these are:

$$\begin{bmatrix} (m_F s^2 + b_F s + k_F + k_I) & -k_I & 0 \\ -k_I & (m_L s^2 + k_T + k_I) & -k_T \\ 0 & -k_T & (b_m s + k_m + k_T) \end{bmatrix} \begin{bmatrix} \delta \\ x_b \\ x_m \end{bmatrix} = \begin{bmatrix} F \\ 0 \\ -\beta \end{bmatrix} \tag{4}$$

Referring to Figure 14 this combined muscle-manipulator element is designated as G_{NMFS}. In Eqn. 4 stick deflection δ replaces c (manipulator position) used in Figure 6, and β (the NM actuation signal) replaces $c_f \Delta f_\alpha$, where for simplification c_f is assumed to be unity and β is the motoneuron signal Δf_α. FS damping, b_F, has been added to the matrix to account for FS viscosity.

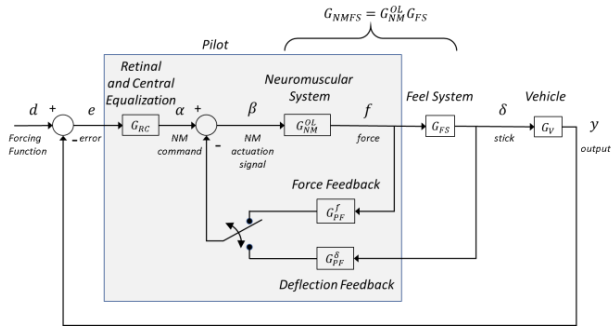

Figure 14. Pilot neuromuscular subsytems.

Solving Eqn. 4 for the manipulator deflection response to β (assuming $F = 0$),

$$G_{NMFS} = \frac{\delta}{\beta} = \frac{k_I k_T}{\Delta}, \quad \text{where}$$

$$\Delta = [(m_L s^2 + k_T + k_I)(b_m s + k_m + k_T) - {k_T}^2] * (m_F s^2 + b_F s + k_F + k_I) - {k_I}^2 (b_m s + k_m + k_T) \tag{5}$$

When the FS mass m_F and damping coefficient b_F are effectively zero, fifth-order Eqn. 5 reduces to third-order (Eqn. 6)

$$\Delta = [(m_L s^2 + k_T + k_I)(b_m s + k_m + k_T) - {k_T}^2] * (k_F + k_I) - {k_I}^2 (b_m s + k_m + k_T) \tag{6}$$

The NM system's basic organization and dynamics for tracking tasks was experimentally validated by Magdaleno (Ref. 6) in 1971, where the NM actuation signal (Figure 35) was directly observed through electromyography (EMG) measurement. EMG is muscle electrical activity in response to a nerve's stimulation of the muscle. Identification of the G_{NMFS} was conducted for two spring-centering manipulator types, a hand manipulator and rudder pedals. Operation of the rudder pedal manipulator involved an inherently balanced agonist/antagonist muscle, producing high quality EMG signal data.

Figure 16 shows time histories of stages of EMG processing associated with rudder pedal deflection. The signal labeled "Difference" is the effective muscle actuation signal β in Figure 14 that was employed to compute operator frequency response. The signal labeled "Smooth Difference" used a first-order lag at 15 rad/s to remove some of the high frequency power to facilitate visual comparison with the pedal position. The trace labeled "Average Tension" is the averaged EMG signal and was highly correlated with the force exerted by each leg on a rudder pedal.

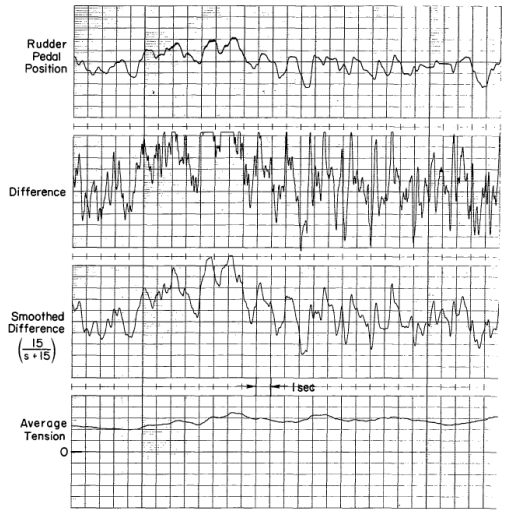

Figure 15. Time history for EMG signal processing (Ref. 6).

Figure 16 shows the frequency response data computed for the rudder pedals and a fitted third-order describing function having a natural frequency of 11 rad/s and a damping coefficient of 0.8.

Despite employing a different muscle group, limb inertia, and manipulator the hand inceptor a produced similar frequency response (although there were some runs that generated a more lightly damped response near 10 rad/s). Since the FS masses for the rudder and hand manipulator were small compared to the spring constants (i.e., the natural frequencies were much higher than 10 rad/s),

and damping forces were low, $G_{NMFS} \approx G_{NM}^{OL}$. From this study it appeared that the human NM system tends to adapt to the FS such that their combination G_{NMFS} exhibits a dominant second-order mode with a damping ratio of 0.7 and a natural frequency near 10 rad/s.

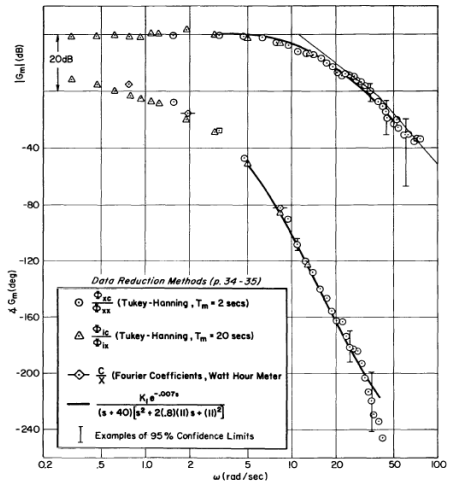

Figure 16. Neuromuscular-feel system (G_{NMFS}) identification data and fitted describing function for rudder pedal control (Ref. 6).

In his Structural Model Hess approximated the open-loop NM element G_{NM}^{OL} (represented as Y_{NM} in Figure 8) as this second-order transfer function and closed the NM loop with the stick position output δ of the FS. In Ref. 25 Hess showed that this modeling approach qualitatively reproduced closed-loop pilot response.

In Ref. 26 Gordon-Smith investigated the effects of manipulator dynamics on human operator response. Figure 17 shows the frequency response data computed in this study for a free moving inceptor (essentially weightless with no restoring spring force) and a pressure stick (a fixed rod with a strain gage). Because the vehicle dynamics being controlled were rate command, the proprioceptive feedback elements in Figure 14 would be gain (no lead or lag) $G_{PF} \approx K_{PF}$. Since G_{FS} is approximately a gain, $G_{NM}^{CL} \propto Y_P$ and the Y_P frequency response in Figure 17 can be equated to G_{NM}^{CL}.

Ref. 6 fitted curves to the data by closing the massless third-order approximation for G_{NMFS} given by Eqn. 6 with the NM feedback loops shown in Figure 5. The spindle feedback element was used with the pressure stick (lead-lag), and the joint sensor feedback element (gain) with the free moving inceptor. Ref. 6 provides mathematical and functional descriptions of the feedback mechanisms employed in limb motion control, and states that although assigned to the spindle sensors in Figure 5, force feedback enlists both the spindle and Golgi ensembles. For modeling manual control their net effect over the mid and high frequency range is adequately reflected by a lead-lag term. Joint angle sensor data indicates this ensemble also acts as a lead-lag but at much lower frequencies such that for the frequency range of interest it can be characterized as a gain and time delay.

In the current work, the response of the two inceptors seen in Figure 17 was emulated using the following procedural steps (control elements are referenced to Figure 14):

1. Assemble the lumped NM-FS model, G_{NMFS}, using known FS parameters and known and assumed limb parameters for the mechanical model shown in Figure 6 and represented by Eqn. 5
2. Extract the open-loop G_{NM}^{OL} using the relation

$$G_{NM}^{OL} = G_{NMFS} G_{FS}^{-1} \tag{7}$$

   and include a NM time delay τ_{NM}
3. Adjust limb parameters k_M, b_M, and k_T until the damping ratio for G_{NM}^{OL} is approximately 0.7 (i.e., the dominant mode exhibits a weak peaking)
4. Compute the closed-loop G_{NM}^{CL} by closing G_{NM}^{OL} with the proprioceptive feedback element

$$G_{PF} = K_{PF} \frac{(s+\omega\_Ld_{PF})}{(s+\omega\_Lg_{PF})} \tag{8}$$

   ($G_{PF} = K_{PF}$ when the vehicle dynamics are rate command)
5. Adjust G_{PF} to match the observed pilot transfer function

$$f/e = Y_P = G_{CR} G_{NM}^{CL} \tag{9}$$

   (If force f is not available use δ/e and include G_{FS})
6. Repeat steps 3 – 5 if needed

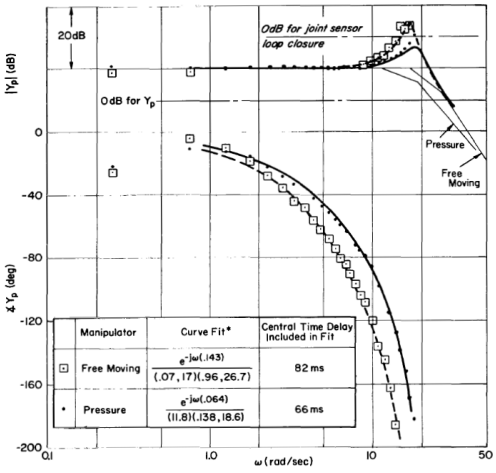

Figure 17. Pilot frequency response ($Y_P = \delta/e$ and $Y_P = f/e$) and fitted describing function for pressure and free moving manipulators;

experimental results from Ref. 26, fit from Ref. 6 (rate command dynamics).

Application of this identification procedure produced Figure 18 and Figure 19 for the pressure and free moving inceptors, and their corresponding parameter values are given in Table *2*. In addition to the excellent agreement in closed-loop magnitude and phase frequency response, the identified neural time delays closely match the delays of the fitted responses shown in Figure 17.

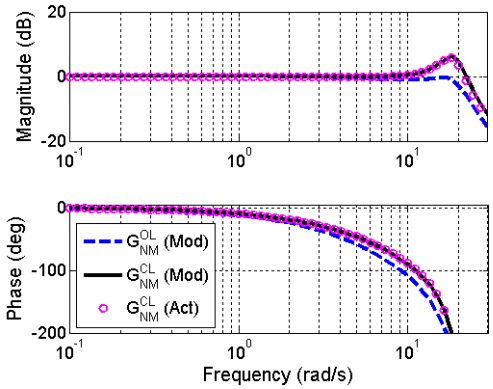

Figure 18. Comparison of actual and modeled closed-loop neuromuscular response (G_{NM}^{CL}); experimental results from Ref. 26 (pressure manipulator, rate command dynamics).

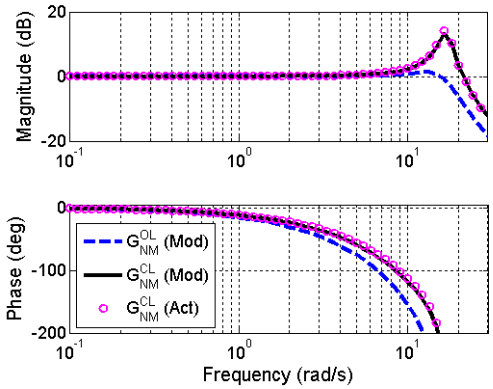

Figure 19. Comparison of actual and modeled closed-loop neuromuscular response (G_{NM}^{CL}); experimental results from Ref. 26 (free moving manipulator, rate command dynamics).

Table 2. Neuromuscular-feel system *(G_{NMFS})* model parameters for pressure and free moving inceptors.

Manipulator Type	Pressure	Free Moving
K_{PF} PF gain	0.5	0.9
k_F (N/m), FS elasticity	10000000	0
b_F (Ns/m), FS viscosity	0	0
m_F (kg), FS mass	0.01	0.01
k_M (N/m), Muscle elasticity	40	80
b_M (Ns/m), Muscle viscosity	9	10
k_T (N/m), Tendon elasticity	120	120
m_L (kg), Limb mass	0.35	0.35
k_I (N/m), Interface elasticity	30	30
τ_{NM} (ms), Neural time delay	60	130

5. FEEDBACK EXPERIMENT

The effect of inceptor force feedback on pitch tracking performance and NM response was explored using a series of simulation runs employing the Microsoft Sidewinder joystick (Figure 20) with and without the pitch axis spring. Three vehicle command types were used for the experiment: proportional ($Y_c = K_c$), rate ($Y_c = K_c/s$), and acceleration ($Y_c = K_c/s^2$). A sum-of-sines (SOS) forcing function containing eleven non-harmonic sine waves was employed where the amplitudes decreased logarithmically (power of 10) with increasing frequency. SOS frequency ranged from 0.048 to 4.65 rad/s, and the length of each run was 60 seconds.

Figure 20. Microsoft Sidewinder joystick.

The compensatory display used is shown in Figure 21, with the objective being to align ownship's symbol with the stationary target.

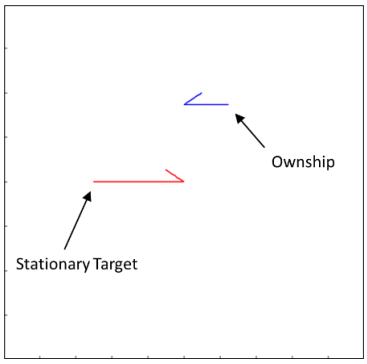

Figure 21. Compensatory tracking display used in force-feedback experiment.

The experiment used a single subject with 1,000 hours of military flight time. Two practice runs were followed by four recorded runs for each of the six conditions shown in Table 3 (three command types, two inceptor dynamics).

Table 3. Force feedback experimental matrix.

Inceptor Dynamics \ Command Type	Prop	Rate	Acc
Free Moving	X	X	X
Spring Centering	X	X	X

6. EXPERIMENTAL RESULTS

Tracking performance for the six conditions is shown in Figure 22, where the standard deviation of the error is normalized by the forcing function's standard deviation (σ_e/σ_i). It is seen that performance significantly degrades ($p < .01$) when the spring gradient is removed during rate and acceleration command control. However, proportional control marginally *improved* (not significantly) when the spring was absent. These results are consistent with a 1966 study (Ref. 5) discussed next.

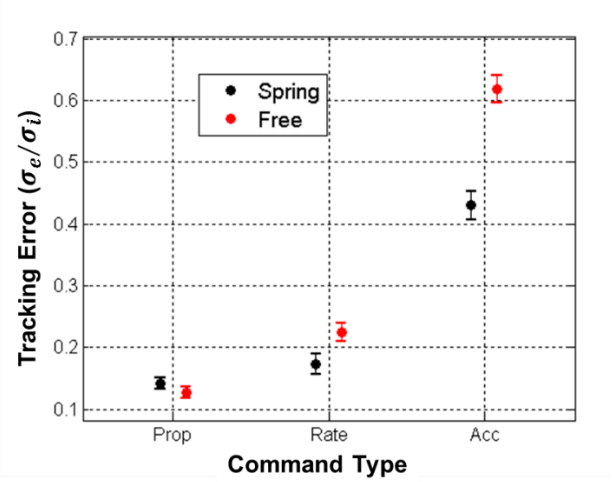

Figure 22. Tracking error by command type for free-moving and spring-centering inceptors (bars denote one standard deviation).

In Ref. 5 STI conducted a battery of experiments examining the effect of manipulator characteristics (spring gradient, inertia, etc.) on tracking performance using two command type control dynamics (proportional and acceleration). Table 4 presents data using proportional command dynamics. The minimum inertia case (I_{min}) highlighted in blue is effectively free moving, and its performance is approximately equal to the two conditions using a spring gradient.

Table 4. Tracking performance for different inceptor conditions (proportional command) Yellow denotes best performance with spring, blue denotes free moving (Ref. 5).

$$Y_c = K_c$$

Configuration	Restraints	K_c	σ_e/σ_i
◊ ㉝	Pressure Controller ($k = 73\,k_I$)	$\frac{73}{5}K_I^*$	0.30
△ ⑩	$I_{min} + 25\,k_I$	K_I	0.28
⊙ ⑧	$I_{min} + k_I$		0.29
⊡ ①	I_{min}		0.27

Acceleration command data is presented in Table 5, where it is seen that the free moving inceptor performs approximately 30% worse than the best-performing spring condition (highlighted in yellow). In Figure 22 the free moving inceptor exhibited 50% more tracking error than the spring-constrained inceptor. Comparing similar conditions, tracking error in Figure 22 was lower than what was observed in Table 4 and Table 5, which was likely due to a lower input bandwidth. However, the trends between the two studies agree quite well.

Table 5. Tracking performance for different inceptor conditions (acceleration command) Yellow denotes best performance with spring, blue denotes free-moving (Ref. 5).

$$Y_c = K_c/s^2$$

Configuration	Restraints	K_c	σ_e/σ_i
⊡ ㉕	Pressure Controller ($73\,k_I$)	$\frac{73}{5}K_a^*$	1.05
△ ⑳	$I_{min} + 25\,k_I$	K_a	1.26
⊙ ⑲	$I_{min} + 5\,k_I$		1.00
⊙ ⑱	$I_{min} + k_I$		1.16
◊ ⑬	I_{min}		1.30

The spectral content of the stick response is now investigated to assess NM feedback path activity (the 1966 STI study did not provide sufficient spectral resolution for such an examination). The highest forcing function frequency used in the force feedback experiment was 4.65 rad/s, and it is assumed stick power beyond this frequency is largely due to NM response. Figure 23 shows the power spectral density (PSD) of a run using spring-centering and rate command dynamics. Well-defined peaks indicate the frequencies of the sum-of-sines (SOS), and beyond the highest SOS frequency there is a cluster of power peaking roughly at 7 rad/ denoted as the NM mode.

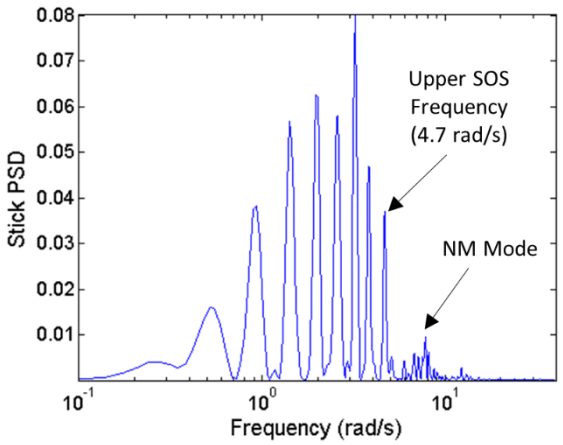

Figure 23. Stick PSD using spring-centering inceptor (rate command dynamics).

In Figure 24 the same rate command dynamics are used, but the inceptor is now free moving. We see

that the stick amplitude relative to the previous run is substantially reduced for both the SOS and NM frequency regions.

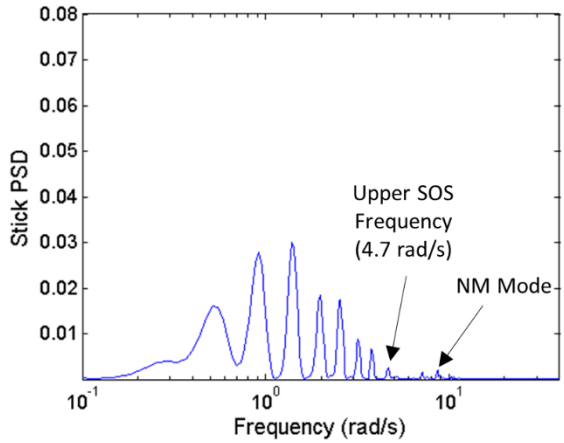

Figure 24. Stick PSD using free moving inceptor (rate command dynamics).

Using the mechanical model (Eqn. 5) to characterize the lumped element G_{NMFS}, parameters associated with the joystick FS and the controlling limbs (thumb and forefinger) produced a closed-loop NM mode near 7 rad/s. Relative to the force generated by the wrist during traditional control of an aircraft cyclic, tension in the thumb and forefinger when operating the joystick is very light. The subsequent low muscle tension/stiffness produced a lower NM mode than the 10 rad/s mode typically observed when conducting manual control using wrist movement with a cyclic. A tracking study (Ref. 21) using a gamepad also identified the NM mode near 7 rad/s, where the controlling limb was the thumb. When fingertip control is used, muscle stiffness is the reciprocal of the sum of the reciprocal stiffnesses of each joint's muscle, so that the net stiffness is very low relative to muscle stiffness corresponding to wrist control.

Ref. 27 measured grip force and muscle stiffness in the wrist during gripping tasks. Plotted in Figure 25, the relationship between the two is approximately linear. This demonstrates that as the exerted force

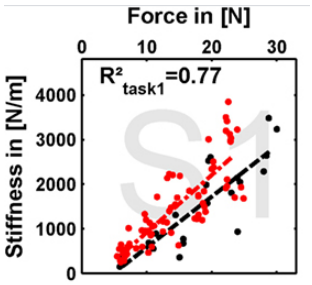

Figure 25. Muscle stiffness versus force (Ref. 27).

decreases, muscle stiffness also decreases. The resistive forces of a gaming joystick and gamepad would generally be less than those of a cyclic or sidestick.

The effect of command type on closed-loop NM (G_{NM}^{CL}) output was simulated using the lead-lag proprioceptive feedback model given in Eqn. 3. Simulated gain, lead and lag values used in the model were based on trends observed from the proprioceptive lead and lag estimates computed from the actual data. The open-loop NM damping ratio and natural frequency were modeled as 0.7 and 7 rad/s, respectively. The simulated frequency response for the three command types is shown in Figure 26, where the amplitude at the NM peak is successively larger moving from proportional to rate and acceleration.

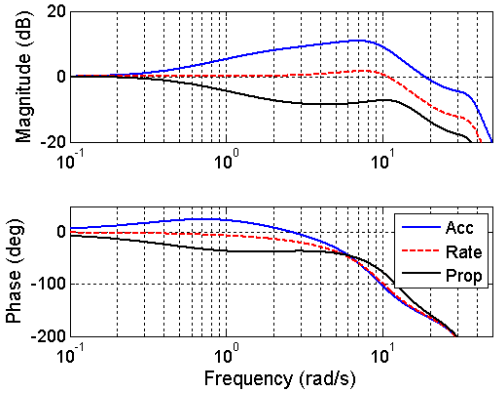

Figure 26. Simulated closed-loop neuromuscular-feel system response for proportional, rate and acceleration command control.

NM stick power is plotted in Figure 27, and consistent with Figure 26 the power rises significantly across command type when the inceptor is spring-centering. Closing the proprioceptive loop around the open-loop NM element (G_{NM}^{OL}) will generally create a second, higher frequency mode associated with the FS. Removing the spring appreciably reduces the NM

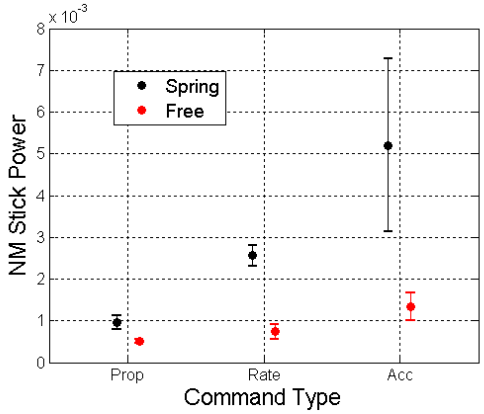

Figure 27. Neuromuscular stick power by command type for free moving and spring-centering inceptors (bars denote one standard deviation).

stick power, i.e., the proprioceptive feedback path is attenuated. This suggests the role of NM equalization changes depending on whether force feedback is present, and that the presence or absence of force feedback influences the role of visual equalization during manual control.

The open-loop NM element (G_{NM}^{OL}) amplitude is largely influenced by the tendon and muscle stiffnesses, k_m and k_T, and muscle damping b_m. Because muscle stiffness is driven by COC, which varies with task and operator intensity, G_{NM}^{OL} is dynamic element. Since k_m directly affects the open-loop NM mode, it is hypothesized that the reduction in relative NM stick power associated with position feedback is primarily due to reduced k_m. This is supported in Figure 28 where the crossover frequencies for the free moving inceptor are significantly lower than the spring-constrained stick for rate and acceleration command. As the joint position sensors only modulate gain, proportional command operation using the free moving stick would likely obtain the necessary lag via the visual channel.

The integral visual equalization element ϵ/s depicted in the SM (Figure 8) accounts for low frequency tracking (well below crossover) of step-like commands. It is proposed that at frequencies in the vicinity of ω_c it is easier to generate lag using the visual channel rather than the proprioceptive one, since the latter requires lead generation (i.e., is more resource-intensive). Generating lag visually would thus allow more efficient use of muscular effort. Hence despite its significantly lower NM stick power, the free moving stick's ω_c is not significantly lower than the spring-centering stick's (the mean ω_c value is actually higher).

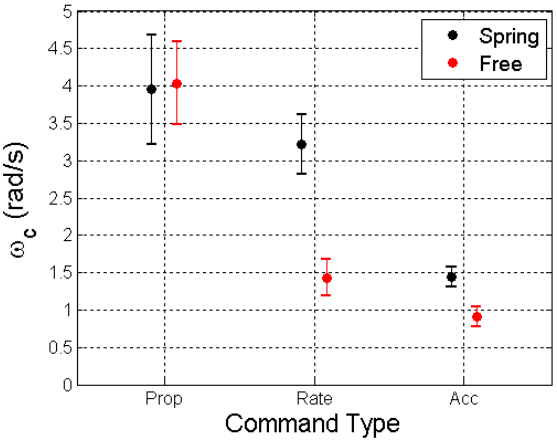

Figure 28. Crossover frequency by command type for free moving and spring-centering inceptors (bars denote one standard deviation).

In Figure 29 phase margin (PM) is not significantly different between the two stick restraint conditions while controlling proportional command. For rate command, the free moving PM is significantly greater than the spring restrained PM. Since the free moving ω_c was half that of the spring's, we see when force feedback is not available that operation is constrained to frequencies such that gain feedback (via positional proprioception) is essentially avoided. A higher ω_c would require higher COC (k_m), which would incur more NM-induced phase loss and require NM compensation - which is largely not available with position feedback.

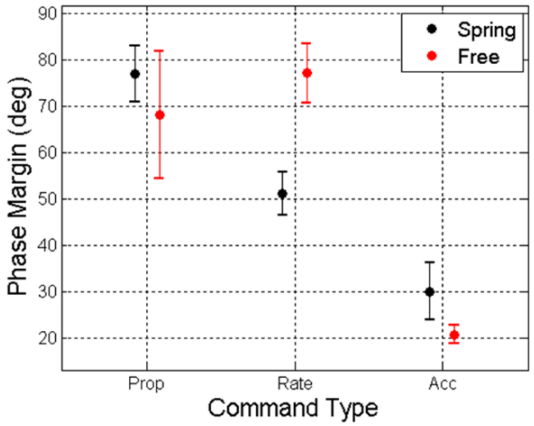

Figure 29. Phase margin by command type for free moving and spring-centering inceptors (bars denote one standard deviation).

Acceleration command requires lead generation in the region of crossover. In Figure 30 there is no significant difference between the spring and free moving open-loop slope for acceleration command. Furthermore, the free moving stick has a 20-degree PM, so that lead is clearly being generated (probably via the visual channel). Visual lead would be a resource-intensive operation, consistent with the free moving stick's significantly lower ω_c and PM compared to the spring-restrained inceptor.

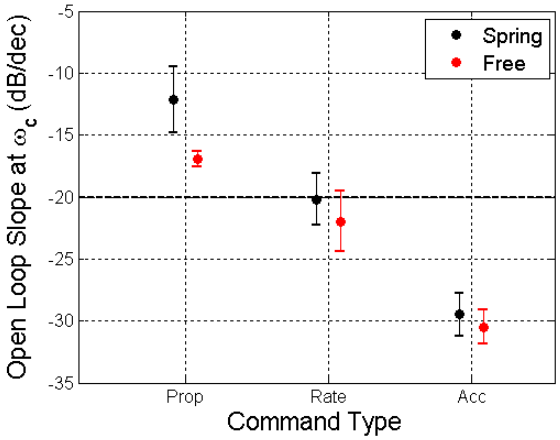

Figure 30. Open-loop slope at ω_c by command type for free moving and spring-centering inceptors (bars denote one standard deviation).

In Figure 31 for both spring and free moving inceptors the open loop (G_{OL}) lead (ω_{Ld}) for acceleration command is commenced at approximately the same frequency (0.6 rad/s), and lead terminates (ω_{Lg}, Figure 33) at approximately 2 rad/s for both of them . Lead would need to extend to roughly 12 rad/s for the open-loop slope to approach -20 dB/dec (the Crossover Model's prediction).

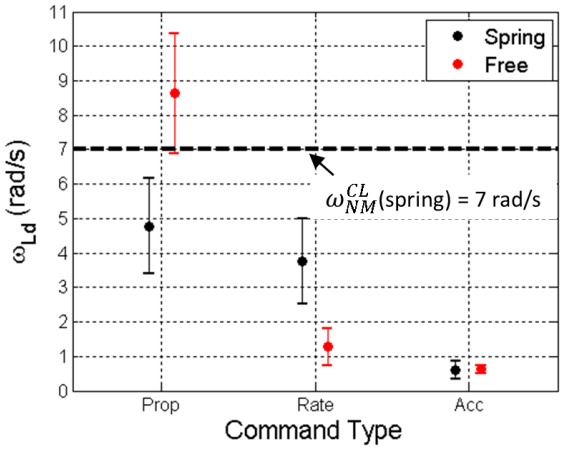

Figure 31. Open-loop lead by command type for free moving and spring-centering inceptors (bars denote one standard deviation).

Looking at the spring-centering stick PSD for acceleration command (Figure 32), we see the NM mode produces substantial power from the last sum-of-sines frequency (4.7 rad/s) out to 10 rad/s. The NM power may even extend below 4.7 rad/s. Frequency compensation such as lead would be difficult if it overlapped with the region of NM power, and it is proposed that the low lag values (yielding open-loop slopes that do not conform to the Crossover Model predictions) arise from a closed-loop NM mode whose frequency is much lower than what was observed for data conforming to the Crossover Model (i.e., approximately 20 rad/s). The reason for the variance in NM mode frequencies is largely attributed to muscle stiffness differences due to limb control (finger-tip versus wrist).

Proportional command control, spring-centering and free moving, produces substantially less NM stick power than acceleration command control (Figure 27). It might be expected that the effect of the NM mode on proportional control would accordingly be less, i.e., frequency compensation can extend closer to or even beyond the NM mode than it did for acceleration command. This anticipated result is seen in Figure 31, where the average effective open-loop lead for the free moving stick (proportional control) is almost 9 rad/s, compared to 5 rad/s for the spring-centering stick.

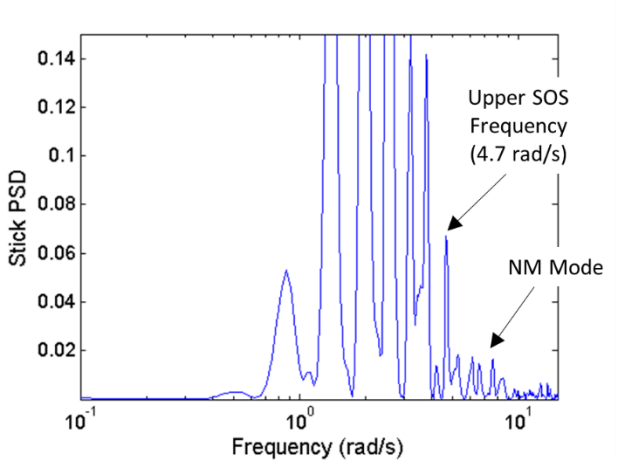

Figure 32. Stick PSD using spring-centering inceptor (acceleration command dynamics).

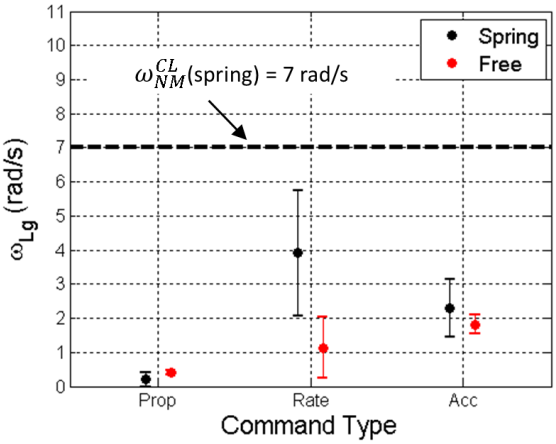

Figure 33. Open-loop lag by command type for free moving and spring-centering inceptors (bars denote one standard deviation).

For proportional command, the free moving stick is producing significantly more lag at crossover than the spring-restrained inceptor, seen from their open-loop slopes in Figure 30. It is proposed that generating lag in the visual channel (free moving inceptor) should be easier than generating lead proprioceptively (required to produce effective lag with the spring-centering stick). Note the free moving stick/proportional command configuration has the smallest variation in open-loop slope compared to the other configurations.

Linear coherence (ρ) is a metric that reflects the degree to which a system behaves in a linear fashion, and a time-domain definition of ρ is defined in Eqn. 10, where a simulated output y_{sim} from a linear model is compared to the actual output y_{act}.

$$\rho = \sqrt{\frac{\sum_1^N (y_{act} - y_{sim})^2}{N}} \Big/ \sigma_{y_{act}} \qquad (10)$$

It is well-established that human operators of dynamic systems prefer to control linear elements (Ref. 8). In Figure 34 linear coherence is significantly *higher* for the free moving stick during proportional command control. This supports the hypothesis that generating open-loop (display-pilot-vehicle suite) lag is an easier operation when conducted via the visual channel compared to using the proprioceptive one when force feedback is available. The stick power results in Figure 27 suggest that the compulsion of force cueing averts the operator from using the visual channel for lag production, despite its apparent advantages.

Linear coherence for the free moving inceptor is lower than the spring-restrained stick for rate and acceleration command (significantly lower for acceleration command). When force is absent and lead is presumably generated through the visual channel (indicated by the low NM response in Figure 27), the reduced linear coherence and its increased variability suggest that visual lead production is a noisy and uncertain process compared to when the open-loop lead is produced proprioceptively using force feedback.

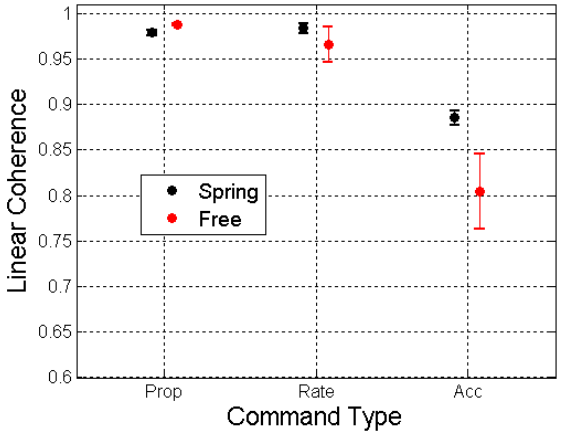

Figure 34. Linear coherence by command type for free moving and spring-centering inceptors (bars denote one standard deviation).

6.1. Closing the NM Loop

The modeled closed-loop NM element should employ the signal which is primarily used as feedback by the pilot. Based on the experimental results presented, force feedback (rather than stick deflection) is thus employed to close the loop (when it is available). This is shown in Figure 35 where a switch closes the loop on the force signal generated by G_{NM}^{OL}, and the FS is distinct from the pilot. When the command type is proportional, three candidate scenarios present themselves. The first is that the pilot generates lag via proprioceptive lead. The second prospective scenario is where the pilot generates direct path lag via the retinal and central equalization element (G_{RC}) and the force feedback element acts as a pure gain to minimize NM-induced phase loss. In both cases Figure 35 holds. The third candidate is where the stick deflection feedback path is used to generate low frequency proprioceptive lead (i.e., effective lag to the direct path), in which case the shaded pilot region in Figure 35 would include the FS.

The key clue as to which is the most likely scenario is provided by the open-loop slope at crossover in Figure 30. When force feedback is removed, there is significantly more lag produced (the slope is closer to -20 dB/dec) than when force is present. The difference in open-loop phase with or without the FS is minimal – only a change in the way equalization is conducted could account for the behavior seen in Figure 30. This suggests that direct path equalization is conducted when force feedback is not available (the second scenario), and when force is present equalization occurs (albeit less effectively) using proprioception.

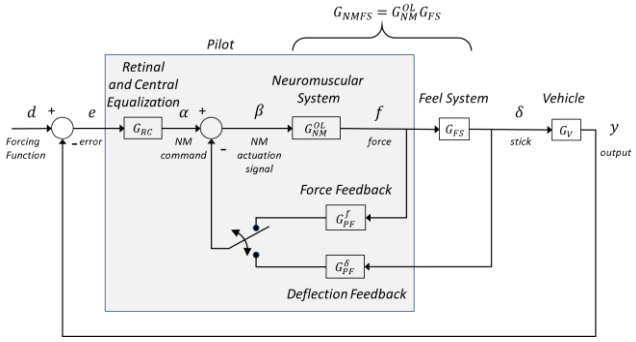

Figure 35. Pilot neuromuscular subsytems (force feedback available).

When force feedback is not present, the FS element is removed as shown in Figure 36 and the feedback switch closes on the stick deflection signal.

When the FS mass and damping forces are minimal compared to the restoring force of the spring (i.e., force is effectively proportional to stick deflection), closing the loop with stick deflection around both G_{NM}^{OL}

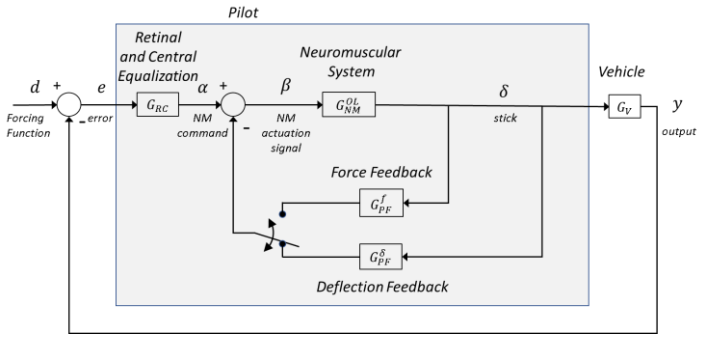

Figure 36. Pilot neuromuscular subsytems (force feedback not available).

and G_{FS} to compute G_{NM}^{OL} is not very different from closing the loop around G_{NM}^{OL} using force. However, closure path selection can have a substantial effect when the mass and/or damping forces are comparable with the spring's forces.

Figure 37 provides an example, where the open-loop NM element G_{NM}^{OL} has a damping ratio of 0.7 and natural frequency of 10 rad/s. The FS damping ratio (ζ_{FS}) and natural frequency (ω_{FS}) used in this example (4.5 and 7 rad/s) was a stick configuration tested on the U.S. Army's JUH-60A RASCAL aircraft. Condition A corresponds to unity gain loop closure around G_{NM}^{OL}, and Condition B to unity gain loop closure around the G_{NM}^{OL} and G_{FS} suite. The difference in phase evaluated at 2 rad/s between the two closure paths is 70 degrees! For a typical FS ($\zeta_{FS} = 0.7$ and $\omega_{FS} = 20$ rad/s, representative of what Hess employed in his analyses), the phase difference between the two loop closure paths is 8 degrees.

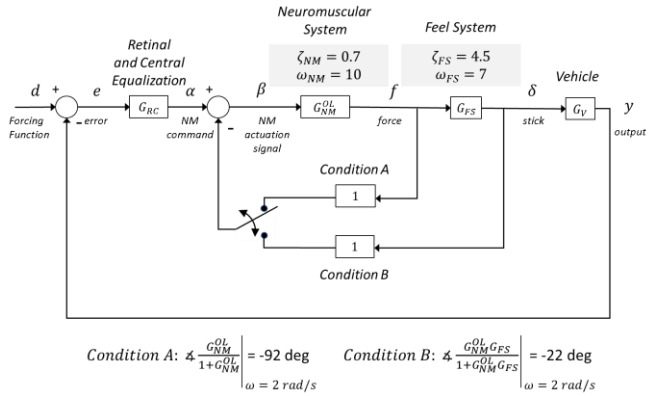

Figure 37. Effect of NM loop closure selection.

Nonetheless, the experimental evidence suggests that when it is available, force (not position) is employed to close the loop on the NM system, and for consistency and accuracy it should be modeled as such.

Reference 28 investigated the relationship between handling qualities rating (HQR) and RASCAL inceptor characteristics while executing Hover and Slalom Mission Task Elements (MTEs). Stick position was used to close the NM loop, however, using force would have produced different analysis results.

6.2. Examining the Relationship Between Crossover Frequency and Stick RMS

In this section the relationship between ω_c and stick root-mean square (RMS) is investigated for the three command types. Stick response δ was simulated using the simple pilot lead-lag model (Eqn. 2) which does not include NM dynamics. Simulated lead and lag values used in the pilot model (ω_{Ld} and ω_{Lg}) were based on trends observed from the lead and lag estimates computed from the actual data. Simulated time delay was also based on estimates computed from the data (note the time delay is not an effective delay which is used in the Crossover Model). Table 6 gives the values used for the simulation. The same sum-of-sines forcing function that drove ownship's symbol in the joystick experiment was also employed.

Table 6. Lead-lag pilot model parameters.

Command Type	Lead (ω_{Ld}, rad/s)	Lag (ω_{Lg}, rad/s)	Time Delay (τ, sec)
Prop	1.5*ω_c	1.2	0.30
Rate	ω_c	ω_c	0.23
Acc	0.4	1.7*ω_c	0.10

The highest sum-of-sines frequency in the forcing function was 4.7 rad/s. Two stick power classifications were defined based on frequency range as follows: *sub_NM* (0 – ω_c), and *NM* (5 – 40 rad/s). The range *sub_NM* is where feedback is effective at reducing tracking error, whereas feedback is ineffective with the latter range. Stick RMS was computed over the range of crossover frequencies that was observed in the experimental data for each command type (Figure 10). In Figure 38 *sub_NM* stick RMS rises fastest with ω_c for acceleration command, with rate and proportional command progressively rising slower (a close-up of the proportional stick RMS response shows a very gradual increase with ω_c).

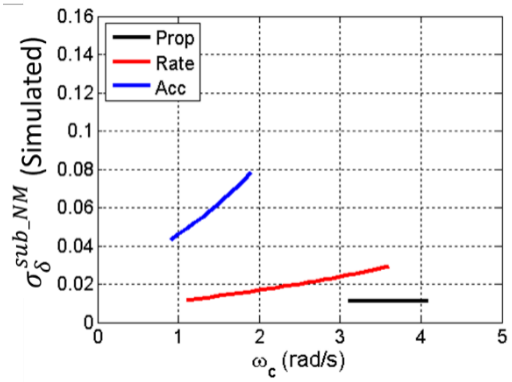

Figure 38. Simulated sub-neuromuscular stick RMS versus crossover frequency.

In Figure 39 actual stick RMS for the *sub_NM* region plotted against ω_c across command type (best-fit lines are computed for each type). The data trends quite well (i.e., similar slope) with the simulated RMS results in Figure 38. The difference in power between actual and simulated would be primarily due to pilot-generated noise (observation, motor, etc.). While actual stick RMS is moderately higher than simulated RMS for both rate and acceleration, it is remarkable how much higher the actual RMS is for proportional command. Despite high noise, proportional

command produced the lowest tracking error, the result of both high ω_c and phase margin as seen in the previous figures.

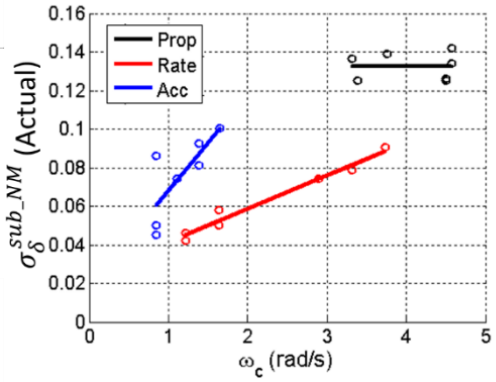

Figure 39. Actual sub-neuromuscular (solid lines are best-fit) and neuromuscular (dotted lines are best-fit) stick RMS versus crossover frequency.

In Figure 40 actual stick RMS for both *sub_NM* and *NM* regions are plotted against ω_c across command type (best-fit lines are computed for each of the six conditions). It is important to observe that the *NM* stick RMS slope mirrors quite closely the *sub_NM* slope, suggesting that the *NM* response is linked to

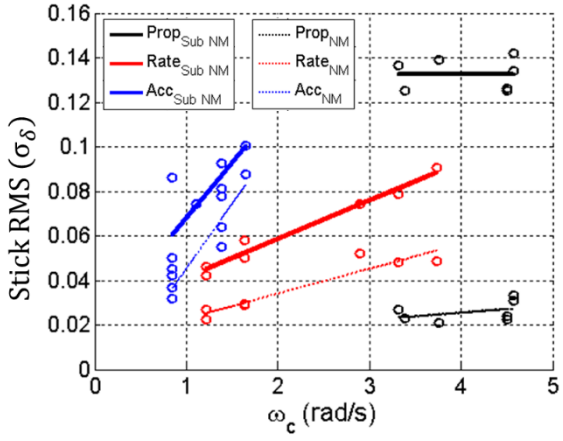

Figure 40. Actual sub-neuromuscular (solid lines are best-fit) and neuromuscular (dotted lines are best-fit) stick RMS versus crossover frequency.

the activity associated with active control. This is confirmed in Table 7 where we see high correlation between the two frequency regions across command type, especially rate and acceleration.

Table 7. Correlation between sub_NM and NM stick RMS across command type.

Command Type	Correlation Between $\sigma_\delta^{sub\_NM}$ and σ_δ^{NM}
Prop	0.71
Rate	0.98
Acc	0.84

The effect of increasing muscle stiffness (arising from COC) on the closed loop NM response is shown in Figure 41 for unity gain NM feedback. Steps 1-4 from the section "NM-Manipulator Dynamics Modeling" were executed while increasing the muscle stiffness k_m (muscle damping b_m and tendon stiffness k_T were also increased as needed to keep the damping ratio of G_{NM}^{OL} approximately 0.7). Note the frequency of the NM mode also increases with muscle stiffness.

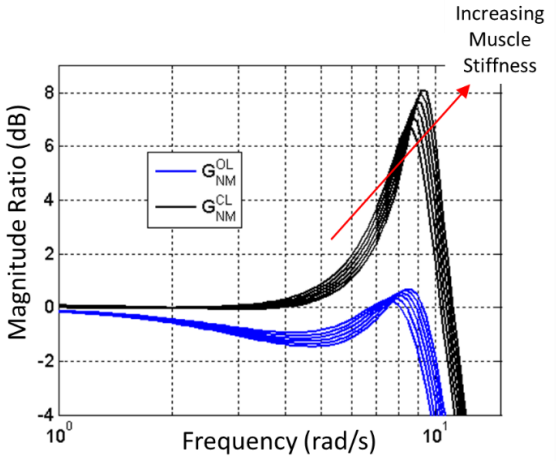

Figure 41. Closed-loop NM response with increasing muscle stiffness.

The experimental data and neurophysiological research presented suggest:

1. Co-contraction (COC) is directly related to muscle stiffness
2. Muscle stiffness is directly related to stick power associated with the frequency region above (supra) active control
3. Supra active control stick power is directly related to the stick power associated with active control (i.e., at and below crossover frequency, ω_c)
4. Active control stick power is directly related to ω_c for a given command type
5. 1-4 infer that COC and ω_c are directly related (a 'high-gain' pilot will generate higher COC than a 'low-gain' pilot.)
6. The active control stick power required to produce a given ω_c results in force power that is driven by the feel system characteristics.

In Figure 42 active control stick power required to produce a given ω_c results in force power that is driven by the feel system characteristics, which in turn drives the requirement for muscle stiffness, setting the requirement for COC. It is proposed that COC is governed by the power of the feel system force required to produce ω_c.

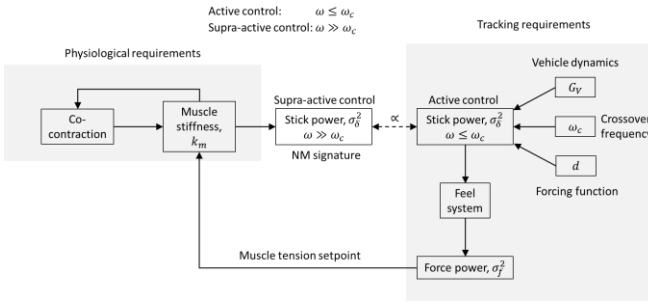

Figure 42. Relationship between tracking and physiological requirements.

7. CONCLUSIONS

It was shown through elementary mechanical modeling how limb-inceptor interaction can influence the NM system. A physical example of this was provided. An experiment using a passive joystick with and without spring restoring force investigated the effect of force feedback on tracking performance and NM response. The preliminary results suggest the role of NM equalization changes depending on whether force feedback is present, and that the presence or absence of force feedback influences the role of visual equalization. When it is available, force (rather than stick deflection) appeared to be the signal employed to close the loop around the NM element. Neurophysiological research and this work's observations suggest that muscle tension arising from limb co-contraction drives operator gain, which in turn governs crossover frequency. This muscle tension affects the mechanical NM response by changing the muscle stiffness and damping.

The fundamental hypothesis of the Structural Model is that the primary equalization characteristics of the human controller (i.e., the generation of needed lead, lag, etc. to yield crossover model characteristics) occurs in proprioceptive rather than visual feedback loops in the human controller. Preliminary data presented in this work indicates that an inceptor that is not spring-centering may offer an advantage in performance and operator workload when controlling proportional command dynamics. It is proposed that generating lag in the visual channel (free moving inceptor) should be easier than generating lead proprioceptively (required to produce effective lag with the spring-centering stick). Proportional command tasks such as attitude tracking (i.e., aerial refueling, formation flight) may thus benefit from this finding.

Figure 43 graphically summarizes the primary concepts developed in this paper surrounding force feedback and the interdependence between the NM system and the FS (fixed base motion is assumed). The Structural Model uses stick deflection as the proprioceptive feedback signal, however the results presented suggest force is employed for feedback when it is available. It was demonstrated that employing deflection feedback can produce large errors in modeled stability margin depending on the feel system dynamics.

Eqn. 5 governs the lumped dynamics representing the suite G_{NMFS}. The operating tension of the limb muscles is set by power of the force required to drive the stick deflection to produce the pilot's desired ω_c. The force is also driven by the forcing function *d* and the FS characteristics. The limb muscle operating tension and limb function sets the limb parameters $k_M, b_M,$ and k_T that comprise Eqn. 5 (G_{NMFS}). Once G_{NMFS} is established, the open-loop NM element G_{NM}^{OL} is computed using the inverse of FS, and a pure time delay τ_{NM} is assigned to G_{NM}^{OL} (approximately 0.06 sec). In general, this element has a damping coefficient that is approximately 0.7, and the dominant mode is primarily a function of limb mass and muscle and tendon stiffness (i.e., loading).

The proprioceptive feedback element G_{PF} provides compensation for G_{NM}^{OL}, G_{FS}, and G_V to satisfy the pilot goals. Ref. 21 models these goals with a cost function which modulates the following four items: 1) Tracking error; 2) Workload; 3) Linearity between workload and PM; and 4) Setting a reference PM. ω_c is a consequence of pilot cost function minimization.

The direct-path equalization element G_{RC} provides low-frequency compensation and is associated with processing time delay τ_{RC} that is a function of the vehicle G_V. Ref. 21observed that lower limits on τ_{RC} exist (again dependent on G_V) to ensure linearity between perceived workload and phase margin. In this way a phase margin setpoint can be used to support loop stability.

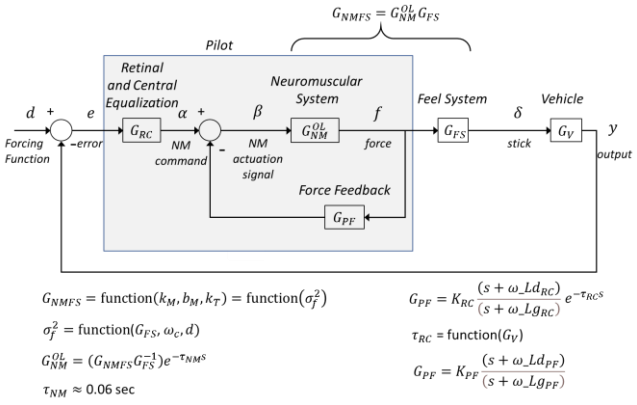

Figure 43. System elements and dependencies for compensatory tracking task (fixed-base operation, deflection sensing control).

Finally, the different NM mode locations associated with wrist and fingertip control appeared to arise from their different muscle stiffnesses (fingertip control employs stiffness elements of each joint that are in

series, which results in very low stiffness and correspondingly lower NM mode frequency). Furthermore, the NM mode location affects the extent that an operator can generate frequency compensation, and the degree to which the Crossover Model is adhered to.

8. ACKNOWLEDGMENTS

This work was supported by cooperative agreement 80NSSC19M0228 between the U.S. Army Technical Development Directorate and San Jose State University.

REFERENCES

1 Goodyear Aircraft Corporation Report GER-4750."Human Dynamic Study." 1952.

2 McRuer, Duane T., Krendel, E. S. "Dynamic Response of Human Operators," Wright-Patterson Air Force Base, Ohio, Rept. No. WADC TR 56-524; 1957.

3 Magdaleno, R. P., Duane T. Mc Ruer, and George P. Moore. "Small perturbation dynamics of the neuromuscular system in tracking tasks." (1968).

4 McRuer, Duane T., Raymond E. Magdaleno, and George P. Moore. "A neuromuscular actuation system model." *IEEE Transactions on Man-Machine Systems* 9.3 (1968): 61-71.

5 Magdaleno, R. E., and Duane T. McRuer. *Effects OF Manipulator Restraints on Human Operator Performance*. Systems Technology Inc. Hawthorne CA, 1966.

6 Magdaleno, Raymond E., and Duane T. Mc Ruer. "Experimental validation and analytical elaboration for models of the pilot's neuromuscular subsystem in tracking tasks." (1971).

7 Tustin, A., "The nature of the human operators response in manual control and its implication for controller design," J. Instn. Elect. Engrs, 94, 190, 1947.

8 McRuer, D. T. and Krendel, E. S., "Mathematical Models of Human Pilot Behavior," No. AGARDograph No. 188, November 1973.

9 Smith, R. H., "A Unified Theory for Pilot Opinion Rating, "Proceedings of the Twelfth Annual Conference on
Manual Control, May 1976, pp. 542-558.

10 R. A. Hess, "A Dual-Loop Model of the Human Controller," J. Guidance Contr., vol. 1, pp. 254-260, July-Aug. 1978.

11 Hess, R. A., "Unified Theory for Aircraft Handling Qualities and Adverse Aircraft-Pilot Coupling", Journal of Guidance, Control, and Dynamics, Vol. 20, No. 6, 1997.

12 Hess, R. A., "Pursuit Tracking and Higher Levels of Skill Development in the Human Pilot", IEEE Transactions on Systems, Man, and Cybernetics, Volume: 11, Issue: 4, April 1981.

13 Krendel, E., McRuer, D., "A servomechanisms approach to skill development," J. Franklin Inst., vol. 269, pp. 24-42, Jan. 1960.

14 McRuer, M., A Neuromuscular Actuation System Model, IEEE TRANSACTIONS ON MAN-MACHINE SYSTEMS, VOL. MMS-9, NO. 3, SEPTEMBER 1968.

15 Hess, R. A., "A Rationale for Human Operator Pulsive Control Behavior," Journal of Guidance, Control, and Dynamics, vol. 2, pp. 221-227, May-June 1979.

16 Hess, R. A., "Unified Theory for Aircraft Handling Qualities and Adverse Aircraft-Pilot Coupling", Journal of Guidance, Control, and Dynamics, Vol. 20, No. 6, 1997.

17 Bachelder, E. N., Aponso, B., "Novel Methods for Estimating Bandwidth and Stability Margins of Pilot-in-Loop Systems ", presented at the 45th European Rotorcraft Forum, Warsaw, Poland, September 17-19, 2019.

18 McRuer, Duane T., and Henry R. Jex. "A review of quasi-linear pilot models." *IEEE transactions on human factors in electronics* 3 (1967): 231-249.

19 Bachelder, E. N., Aponso, B., "Operational Basis for Crossover Model Conformance During Compensatory Tracking", presented at AIAA Atmospheric Flight Mechanics Conference, 2021.

20 Bachelder, E. N., Aponso, B., "Operational Basis for Crossover Model Conformance During Compensatory Tracking", presented at AIAA Atmospheric Flight Mechanics Conference, 2021.

21 Bachelder, Edward, and Bimal Aponso. "A Theoretical Framework Unifying Handling Qualities, Workload, Stability, and Control." *Vertical Flight Society 77th Annual Forum & Technology Display, Virtual*. 2021.

22 Gribble, Paul L., et al. "Role of cocontraction in arm movement accuracy." Journal of neurophysiology 89.5 (2003): 2396-2405.

23 Saliba, C. M., Rainbow, M. J., Selbie, W. S., Deluzio, K. J., & Scott, S. H. "Co-contraction uses dual control of agonist-antagonist muscles to improve motor performance." *bioRxiv* (2020).

24 Damveld, Herman, et al. "Identification of the feedback components of the neuromuscular system in a pitch control task." *AIAA Modeling and Simulation Technologies Conference*. 2013.

25 Hess, Ronald A. "Analyzing manipulator and feel system effects in aircraft flight control." *IEEE Transactions on Systems, Man, and Cybernetics* 20.4 (1990): 923-931.

26 Gordon-Smith, M. "An Investigation into Some Aspects of the Human Operator Describing Function While Controlling a Single Degree of Freedom." *NASA Special Publication* 215 (1970): 203

27 Höppner, Hannes, et al. "Key insights into hand biomechanics: human grip stiffness can be decoupled from force by cocontraction and predicted from electromyography." *Frontiers in neurorobotics* 11 (2017): 17.

28 Malpica, Carlos, and J. Lusardi. "Handling qualities analysis of active inceptor force-feel characteristics." *AHS 69th Annual Forum, AHS International*. 2013.